© 2023. Published by The Company of Biologists Ltd | Journal of Cell Science (2023) 136, jcs260771. doi:10.1242/jcs.260771

RESEARCH ARTICLE

A genome-wide genetic screen identifies CYRI-B as a negative regulator of CEACAM3-mediated phagocytosis

Johannes W. P. Kuiper[1], Julia Krause[1], Leon Potgeter[1], Jonas Adrian[1,*] and Christof R. Hauck[1,2,‡]

ABSTRACT

Opsonin-independent phagocytosis mediated by human carcinoembryonic antigen-related cell adhesion molecule 3 (CEACAM3) has evolved to control a subset of human-restricted bacterial pathogens. CEACAM3 engagement triggers rapid GTP-loading of the small GTPase Rac as a master regulator of cytoskeletal rearrangements and lamellipodia-driven internalization. To identify components of the CEACAM3-initiated signaling cascade, we performed a genome-wide CRISPR/Cas9-based screen in human myeloid cells. Following infection with fluorescently labeled bacteria, cells exhibiting elevated phagocytosis (gain-of-function) as well as cells showing reduced phagocytosis (loss-of-function) were sorted and enrichment of individual single-guide RNAs (sgRNAs) was determined by next generation sequencing. Concentrating on genes whose targeting by three distinct sgRNAs consistently resulted in a gain-of-function phenotype, we identified the Rac-GTP-sequestering protein CYRI-B as a negative regulator of CEACAM3-mediated phagocytosis. Clonal HL-60 cell lines with CYRI-B knockout showed enhanced CEACAM3-downstream signaling, such as Rac GTP loading and phosphorylation of PAK kinases, leading to increased phagocytosis of bacteria. Complementation of the CYRI-B knockout cells reverted the knockout phenotype. Our results unravel components of CEACAM3-initiated opsonin-independent phagocytosis on a genome-wide level and highlight CYRI-B as a negative regulator of CEACAM3-initiated signaling in myeloid cells.

KEY WORDS: CEACAM, GTPase, Rac, Phagocytosis, Pathogenic bacteria

INTRODUCTION

Phagocytosis is a critical cellular defense mediated by professional phagocytes including granulocytes, macrophages and dendritic cells. Dedicated phagocytic receptors, such as Fc-receptors, complement receptors, scavenger receptors, CEACAM3 and Dectin-1 (also known as CLEC7A) play an important initiating role in this process (Janeway and Medzhitov, 2002). Whereas Fc-receptors and complement receptors require prior opsonization, CEACAM3 and Dectin-1 directly bind to specific surface-exposed features of their target particles (Underhill and Ozinsky, 2002; Goodridge et al., 2012). In contrast to Dectin-1, which recognizes conserved glycan moieties exposed on the yeast cell wall, CEACAM3 detects a particular functionality of various human-restricted bacterial pathogens – the possession of CEACAM-binding adhesins (Pils et al., 2008). Indeed, the ability to engage members of the human CEACAM family has evolved independently in multiple bacterial lineages, as evidenced by the structurally diverse CEACAM-binding adhesins expressed on the surface of the respective pathogens (Tchoupa et al., 2014). Most of these CEACAM-binding adhesins recognize homologs of CEACAM3 abundantly expressed on epithelia, such as CEACAM1 and CEA (also known as CEACAM5) (Kuespert et al., 2006; Beauchemin and Arabzadeh, 2013). In contrast, the product of the *CEACAM3* gene is only present on granulocytes, and bacterial adhesins seem to be selected to avoid recognition by this receptor (Bonsignore et al., 2019). Accordingly, CEACAM3 is involved in a molecular arms race with specialized human-restricted bacterial pathogens such as *Neisseria gonorrhoeae* (Adrian et al., 2019; Bonsignore et al., 2019). Similar to other CEACAM family members, the extracellular IgV-like domain of CEACAM3 is responsible for binding microbial adhesins, including the Opa proteins of *Neisseria gonorrhoeae* (Schmitter et al., 2004; Roth et al., 2013; Hill and Virji, 2003; Tchoupa et al., 2015; Koniger et al., 2016). However, the functionality of CEACAM3 as a phagocytic receptor depends on a short amino acid sequence in its cytoplasmic domain reminiscent of an immunoreceptor tyrosine-based activation motif (ITAM). Phosphorylation of this motif by Src family protein tyrosine kinases (PTKs) allows recruitment of the SH2-domain containing Rac guanine nucleotide exchange factor Vav (McCaw et al., 2003; Schmitter et al., 2004; Schmitter et al., 2007). As a consequence, CEACAM3 engagement results in a rapid increase in GTP-loaded Rac, activation of p21-activated kinase (PAK), and WAVE-complex-dependent cytoskeletal rearrangements driving the formation of prominent lamellipodia (Hauck et al., 1998; Billker et al., 2002; Schmitter et al., 2004; Pils et al., 2012; Buntru et al., 2012). Stimulation of CEACAM3 is also linked to the production of reactive oxygen species and release of cytokines by granulocytes (Sarantis and Gray-Owen, 2007; Buntru et al., 2011; Sarantis and Gray-Owen, 2012; Heinrich et al., 2016). Therefore, CEACAM3-triggered signaling has to be tightly controlled to prevent excessive inflammation, but cellular regulators of this signaling pathway are poorly characterized.

To identify potential regulatory elements of CEACAM3-initiated phagocytosis, we performed a genome-wide CRISPR/Cas9 screen in human phagocytes. Concentrating on genes that consistently produced a gain-of-function phenotype when depleted by three independent sgRNAs, we identified the Rac-GTP-binding protein CYRI-B as a prominent negative regulator of CEACAM3-driven signaling events. CYRI-B sequesters GTP-bound Rac, thereby limiting Rac-driven downstream processes such as activation of PAK kinases and lamellipodia formation (Fort et al., 2018; Shang et al., 2018; Yuki et al., 2019; Le et al., 2021). We found that

[1]Lehrstuhl Zellbiologie, Fachbereich Biologie, Universität Konstanz, 78464 Konstanz, Germany. [2]Konstanz Research School Chemical Biology, Universität Konstanz, Konstanz, Germany.
*Present address: Cilag AG - JSC Schaffhausen, Hochstrasse 201, 8200 Schaffhausen, Switzerland.

‡Author for correspondence (christof.hauck@uni-konstanz.de)

C.R.H., 0000-0002-1005-2141

Handling Editor: Michael Way
Received 1 November 2022; Accepted 21 April 2023

Journal of Cell Science (2023) 136, jcs260771. doi:10.1242/jcs.260771

knockout of CYRI-B allowed increased phagocytosis of CEACAM3-binding bacteria, which was reverted by re-expression of wild-type, but not Rac-binding-deficient, CYRI-B. These findings not only validate the genome-wide screening approach, but also reveal an unexpected additional layer of Rac regulation in myeloid cells, which could serve as a target to control excessive granulocyte activation.

RESULTS

A genome-wide sgRNA-screen to interrogate CEACAM3-mediated phagocytosis

As a pre-requisite to a genome-wide lentivirus-based screen, the transduction efficiency and phenotypic knockout kinetics of the used cell model have to be evaluated and optimized. Therefore, we screened several human myeloid cell lines commonly employed as granulocyte surrogates for their susceptibility to lentiviral transduction using a GFP-encoding recombinant lentivirus. Although 40–50% of NB4 cells and JOSK-M cells (a subline of U937 cells) became GFP-positive 3 days after lentiviral transduction, the transduction efficiency seen with HL60 cells was >90% (Fig. S1A). Furthermore, the expression of GFP from the lentiviral construct was several-fold higher in HL60 cells, as evidenced by the elevated mean fluorescence intensity (MFI) of the transduced HL60 cell population (Fig. S1A). Accordingly, we turned our attention to HL60 cells and generated a stable HL60 cell line expressing the blue-fluorescent protein Cerulean (HL60 Cer) (Fig. S1B). These cells were transduced with a lentivirus encoding the Cas9 enzyme, a sgRNA targeting the Cerulean coding sequence, as well as a puromycin resistance cassette. At 3 days after viral infection, the cells showed unaltered Cerulean fluorescence (Fig. S1B). At that point, the infected cell population was incubated with puromycin to select for stably transduced cells (Fig. S1B). After 3 days of puromycin selection, a small population of Cerulean-negative cells was observed, which after a further 2 days of puromycin selection amounted to ∼20% of the cell population (Fig. S1B,C). HL60 cells express only low amounts of CEACAM3 and express additional CEACAM family members, including CEACAM1, CEACAM4, CEACAM6 and CEACAM8 (Skubitz et al., 1996; Delgado Tascon et al., 2015; Goob et al., 2022). To maximize CEACAM3-mediated phagocytic events, we therefore stably introduced a CEACAM3–mKate fusion protein (Fig. 1A). The resulting HL60 CEACAM3 cells exhibited rapid opsonin-independent phagocytosis of CEACAM3-binding *Neisseria gonorrhoeae* (Ngo Opa_{52}) as indicated by the shift in cell-associated CFSE-fluorescence derived from internalized CFSE-labeled bacteria (Fig. 1B). In contrast, CEACAM1-binding (Ngo Opa_{54}) or non-CEACAM-binding (non-opaque; Opa^-) gonococci (Ngo Opa^-) were hardly internalized under these conditions (Fig. 1B). At a low multiplicity of infection (MOI), when phagocytosis was not saturated, more than 40% of HL60 CEACAM3 cells had phagocytosed CEACAM3-binding bacteria within 15 min of infection (Fig. 1B; Fig. S1D). Furthermore, HL60 CEACAM3 cells infected with Opa_{52}-expressing gonococci, but not with non-opaque (Opa^-) or Opa_{54}-expressing bacteria, exhibited prominent lamellipodia, as reported for CEACAM3-mediated uptake by granulocytes (Schmitter et al., 2004; Goob et al., 2022) (Fig. 1C). Accordingly, we employed HL60 CEACAM3 cells together with a genome-wide library of single-guide RNAs (sgRNAs) in the lentiviral vector lentiCRISPR v2 (Sanjana et al., 2014) to screen for factors modifying the opsonin-independent phagocytosis via CEACAM3. The layout of the screen is depicted in Fig. 1D. To this end, the HL60 CEACAM3 cells were transduced with the Human CRISPR Knockout Pooled Library (GeCKov2; part A) targeting 19,000 human genes with three different sgRNAs each. After 3 days, the virus-infected cells were selected with 0.3 µg puromycin for 5 days, and an aliquot of the puromycin-resistant HL60 CEACAM3 cell population was set aside (‘Input’). Next, cells were infected at an MOI of 10 for 15 min with CSFE-labeled Opa_{52}-expressing *N. gonorrhoeae* and, upon gating on infected cells, a high-fluorescence population (‘High’) with an above-average phagocytosis and a corresponding low-fluorescence sample (‘Low’) with a below-average uptake of CEACAM3-binding bacteria was collected by cell sorting. Genomic DNA from the Input, High and Low samples was used to amplify the integrated sgRNA and to subject the amplicons to next generation sequencing. Comparison of the relative abundance of specific sgRNAs in the high or low population compared to the input sample was conducted to reveal genes that influence CEACAM3-mediated phagocytosis.

Identifying potential regulators of CEACAM3-mediated phagocytosis

Following the procedure outlined in Fig. 1D, we infected the lentivirally transduced and puromycin-treated HL60 CEACAM3 cell population with an MOI of 10 CSFE-labeled Opa-negative gonococci (Ngo Opa^-), Opa_{52}-expressing *N. gonorrhoeae* (Ngo Opa_{52}), or left them uninfected (Fig. 2A). As expected, Opa_{52}-expressing *N. gonorrhoeae* were readily phagocytosed, whereas Opa-negative bacteria showed no increased signal compared to the uninfected control, indicating that phagocytosis was strictly mediated by the Opa–CEACAM interaction (Fig. 2A). After 15 min of phagocytosis, we collected a total of 3×10^6 cells from a Low population representing the cells within the lowest 20% percentile of fluorescence intensity (Fig. 2B). Furthermore, 2×10^6 cells of a High population were collected, representing the cells within the highest 20% percentile of fluorescence intensity, which indicates above average phagocytosis (Fig. 2B). Re-analysis of the sorted cell populations indicated that the Low population on average contained only ∼50% of phagocytosed bacteria, while the High population on average phagocytosed ∼130% of CFSE-labeled Opa_{52}-expressing gonococci compared to the input population (Fig. 2B). Sequencing of the sgRNA repertoire encoded by cells of the Input, Low and High populations (>16,000,000 reads/sample) allowed us to obtain a quantitative estimate of the relative distribution of individual sgRNAs in the low and high populations compared to the input population. There were 14 sgRNA targets that showed a >2-fold enrichment in the Low population and a depletion (<1) in the High population relative to the Input for all three sgRNAs targeting the same gene. These sgRNA target genes could encode proteins with a positive contribution to CEACAM3-mediated phagocytosis. The ten top hits from this list are depicted in Fig. 2C and encode proteins with a role in vesicle trafficking (RABGGTA), chromatin regulation (SMARCA2) and nucleotide synthesis (PRPS1L1), as well as transmembrane proteins, such as TMEM185A, prominin 1, also known as CD133 (PROM1), the Golgi protein GORASP1 and the zinc transporter SLC39A6. Similar to the signal peptidase (SPCS3), these proteins might have an indirect role in facilitating CEACAM3 processing or transport to the membrane and thereby impact CEACAM3-mediated phagocytosis. A direct connection to CEACAM3-mediated phagocytosis is plausible for proteins such as spectrin A1 (SPTAN1) or the Rac guanine nucleotide exchange factor Dock 3 (DOCK3), which might be involved in the cytoskeletal re-arrangements accompanying bacterial uptake by CEACAM3.

Journal of Cell Science (2023) 136, jcs260771. doi:10.1242/jcs.260771

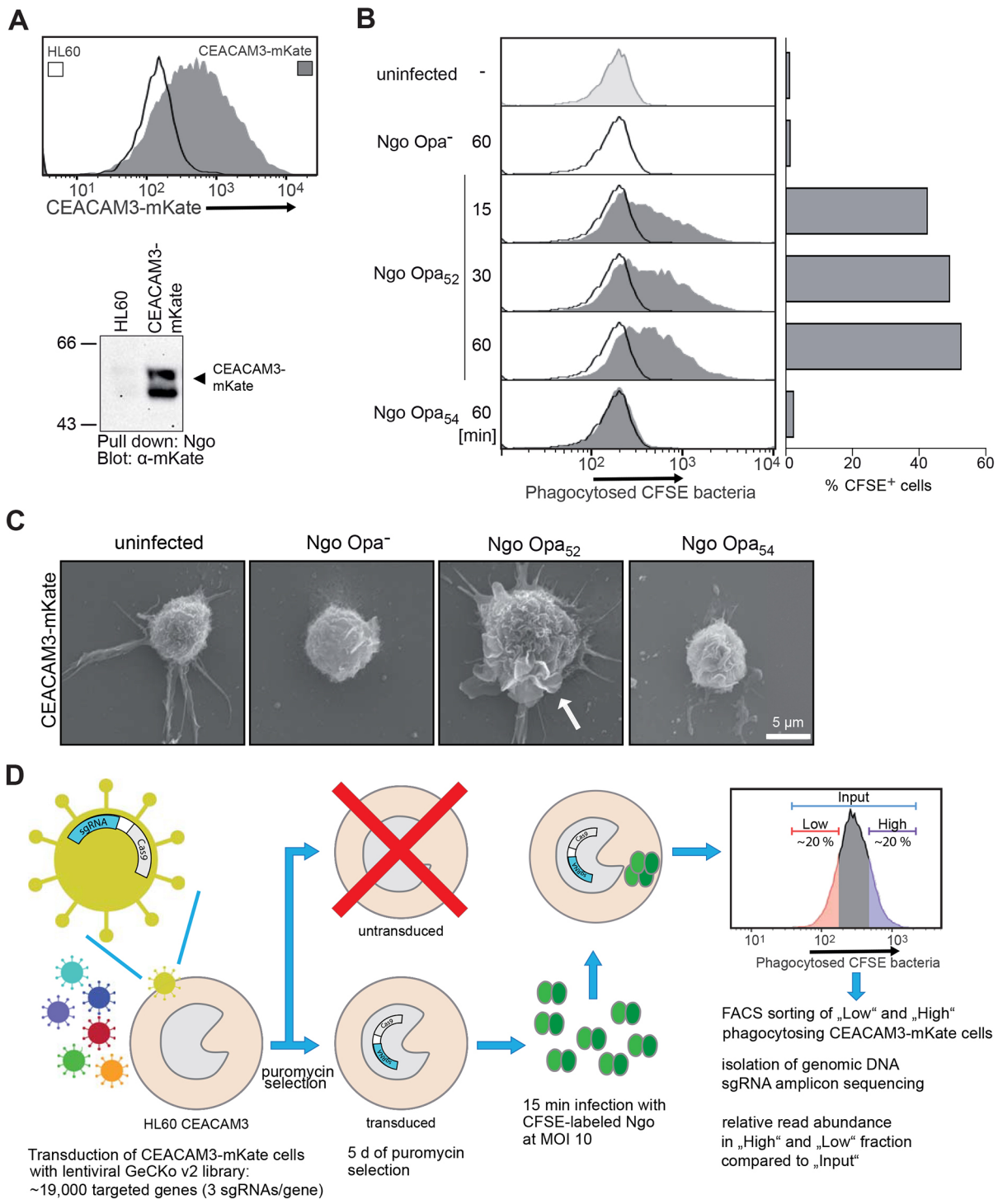

Fig. 1. A genome-wide sgRNA-screen to interrogate CEACAM3-mediated phagocytosis. (A) HL60 cells were stably transduced with CEACAM3–mKate and expression was detected by means of mKate fluorescence by flow cytometry (shaded curve in upper panel). The HL60 parent cell line did not show mKate fluorescence (transparent curve in upper panel). Expression of CEACAM3–mKate was also detected by western blotting with an anti-mKate antibody upon CEACAM pulldown from whole cell lysates using CEACAM-binding *Neisseria gonorrhoeae* (Ngo) (lower panel). (B) HL60 CEACAM3–mKate cells were left uninfected or infected for the indicated time points with CFSE-labeled bacteria: Ngo expressing Opa_{52} (binding to CEACAM1 and CEACAM3), Ngo expressing Opa_{54} (binding to CEACAM1) or with Ngo lacking Opa expression (Opa^-). Phagocytosis was quantified by determining fluorescence of intracellular bacteria by flow cytometry. The bars in the right panel indicate the percentage of CFSE-positive HL60 CEACAM3–mKate cells harboring phagocytosed bacteria. (C) HL60 CEACAM3–mKate cells were infected for 15 min as in B. Samples were fixed and processed for scanning electron microscopy. The white arrow points to prominent lamellipodia induced by CEACAM3-binding bacteria. Images in A–C representative of a single experiment. (D) Scheme depicting the workflow of the genome-wide screen using HL60 CEACAM3–mKate cells and lentiviral transduction with the GeCKo v2 library. Upon infection with CFSE-labeled Ngo, the transduced phagocytes are sorted into a low fluorescent and high fluorescent population. Abundances of sgRNA sequences in the ‘high’ and ‘low’ CFSE populations relative to the ‘input’ population can be determined by next-generation sequencing.

Journal of Cell Science (2023) 136, jcs260771. doi:10.1242/jcs.260771

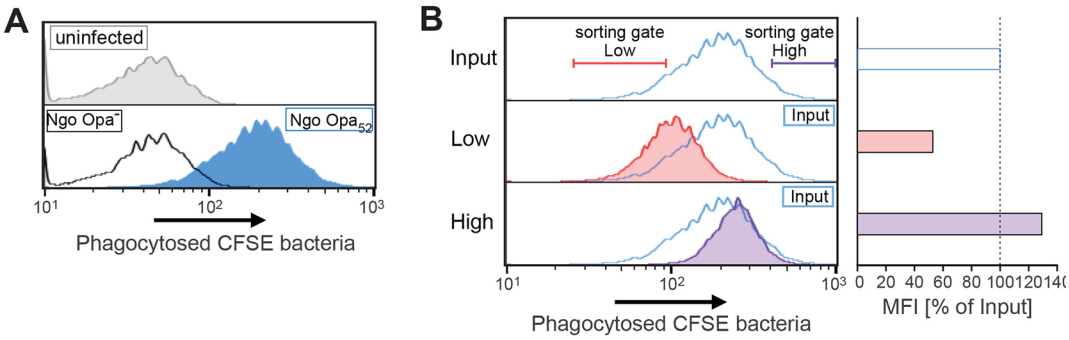

C

Rank	Gene name	Enrichment in "Low"	Enrichment in "High"	GeneID
1	RABGGTA	3.1	0.6	5875
2	SLC39A6	2.9	0.4	25800
3	TMEM185A	2.8	0.6	84548
4	SPCS3	2.7	0.8	60559
5	PROM1	2.5	0.6	8842
6	DOCK3	2.3	0.6	1795
7	SPTAN1	2.3	0.6	6709
8	GORASP1	2.1	0.9	64689
9	SMARCA2	2.1	0.5	6595
10	PRPS1L1	2.1	0.8	221823

Rank	Gene name	Enrichment in "High"	Enrichment In "Low"	GeneID
1	LRIG2	4.9	0.3	9860
2	CYRIB	3.5	0.7	51571
3	HAPLN2	3.3	0.6	60484
4	MEF2BNB	3.1	0.2	729991
5	DNAJC19	3.0	0.6	131118
6	FGFRL1	2.7	0.6	53834
7	S1PR4	2.7	0.5	8698
8	TRO	2.4	0.5	7216
9	TRIM61	2.3	0.6	391712
10	NBEAL2	2.3	0.7	23218

Fig. 2. Identifying potential regulators of CEACAM3-mediated phagocytosis. (A) HL60 CEACAM3–mKate cell population transduced with the GeCKo v2 lentiviral library was left uninfected (upper panel, gray curve) or infected for 15 min with either CFSE-labeled *N. gonorrhoeae* expressing Opa_{52} (Ngo Opa_{52}; lower panel, blue curve) or with non-opaque gonococci (Ngo Opa^{-}; lower panel, black line). Phagocytosis was analyzed by flow cytometry. A fraction of the Ngo Opa_{52}-infected cells was set aside (input population). (B) Ngo Opa_{52} infected cells from A were sorted based on low or high CFSE fluorescence as indicated by the lines depicting the sorting gates. The blue line marks the CFSE-fluorescence distribution of the input population as in A. After sorting, a fraction of the input, the 'low' and the 'high' populations were re-analyzed and the mean fluorescence intensity (MFI) of each population is depicted in the bar graph on the right side relative to the MFI of the input population. (C) Top-10 ranked genes, where all three sgRNAs targeting this gene were found to be enriched in the 'low' population, while showing reduced relative abundance in the 'high' population. This pattern indicates a positive contribution of the gene product to CEACAM3-mediated phagocytosis (left panel). The right panel lists the Top-10 ranked genes, where all three sgRNAs targeting this gene were enriched in the 'high' population, while having at the same time a reduced relative abundance in the 'low' population. This pattern indicates a negative role of the gene product in CEACAM3-mediated phagocytosis (right panel). A detailed description of the analysis is provided in the Materials and Methods section. Images in this figure representative of a single experiment.

We also applied the same algorithm to identify sgRNAs that showed a >2-fold enrichment in the High population and a depletion (<1) in the Low population for all three sgRNAs targeting the same gene. Thereby, we identified 29 sgRNA targets, which could have a negative impact on CEACAM3-mediated phagocytosis and whose depletion should lead to a gain-of-function phenotype. The ten top hits from this list are depicted in Fig. 2C and encode proteins with a role in receptor tyrosine kinase signaling (fibroblast growth factor receptor like 1; FGFRL1) and inhibition (LRIG2), lipid signaling (S1PR4), maturation of secretory vesicles (NBEAL2), lysosome positioning (BLOC-1-related complex subunit 8; MEF2BNB), and regulation of the GTPase Rac (CYRI-B). In these cases, a link to activation of myeloid cells and phagocytosis can be easily envisioned. On the other hand, a potential negative impact of DNAJC19 (protein import in mitochondria), TRIM61 (a ubiquitin E3-ligase), trophinin (TRO; cell–cell adhesion protein), and hyaluronan and proteoglycan link protein 2 (HAPLN2; extracellular matrix assembly) on CEACAM3-initiated processes is not easy to reconcile. Accordingly, it is instrumental to confirm and investigate the connection of these putative factors to CEACAM3-mediated phagocytosis in more detail.

Knockout of CYRI-B in myeloid cells results in a gain-of-function with regard to phagocytosis

To get a first idea of whether the genome-wide screen yielded meaningful hits, we concentrated on CYRI-B (also termed FAM49B). CYRI-B, the CYFIP-related Rac interactor B, bears similarity to the WAVE-complex protein CYFIP, and binds GTP-loaded Rac. Thereby, CYRI-B sequesters GTP-Rac and impedes Rac-dependent cellular processes (Fort et al., 2018; Shang et al., 2018). To this end, we produced clonal CYRI-B knockout lines derived from HL60 CEACAM3 cells. Cells were transduced with lentivirus encoding Cas9 and sgRNAs targeting the critical exon of CYRI-B in the 3′-vicinity of the ATG start codon (Fig. 3A). Transduced cells were selected for 7 days in puromycin and single-cell-derived clonal lines were expanded. Several independent cell lines showed either partial or complete loss of CYRI-B protein expression by western blotting (Fig. 3B). Importantly, clonal line C6 with a complete knockout of CYRI-B retained equivalent total expression and surface localization of CEACAM3 compared to the control transfected cells (Fig. S2). Next, HL60 CEACAM3 cells and HL60 CEACAM3 CYRI-B knockout clone 6 cells (CYRI-B ko) were infected for 15 min with CFSE- and biotin-labeled gonococci, and phagocytosis was evaluated by differential staining of intracellular and extracellular bacteria followed by immunofluorescence microscopy (Fig. 3C). As expected, both HL60 cell lines did not internalize non-opaque bacteria (Fig. 3C). However, Opa_{52}-expressing gonococci were taken up by HL60 CEACAM3 cells, and disruption of CYRI-B expression in CYRI-B ko cells resulted in a more than doubling of the number of internalized bacteria (Fig. 3C,D). This striking gain-of-function was verified by flow cytometry-based analysis of phagocytosis

Journal of Cell Science (2023) 136, jcs260771. doi:10.1242/jcs.260771

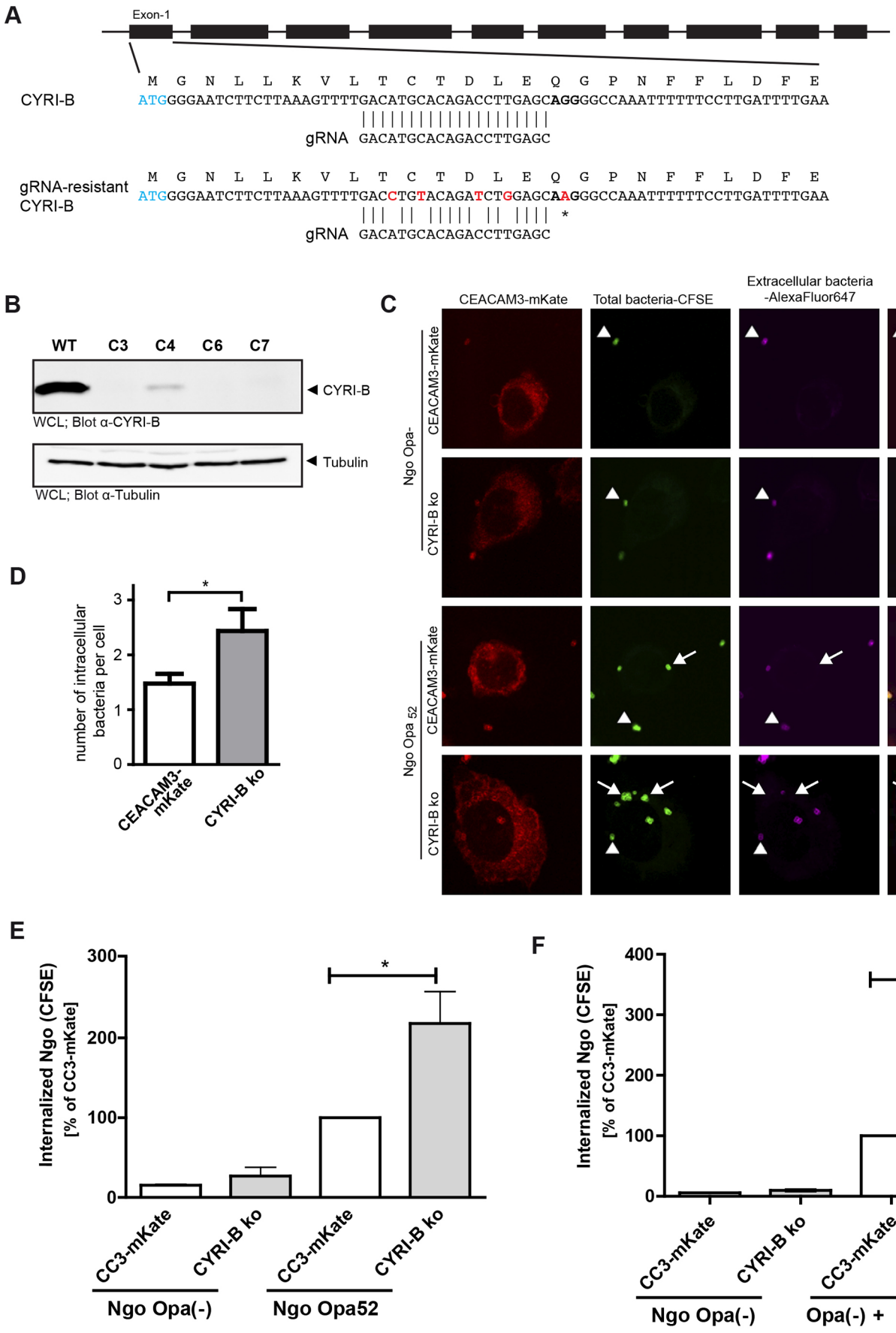

Fig. 3. See next page for legend.

Journal of Cell Science (2023) 136, jcs260771. doi:10.1242/jcs.260771

Fig. 3. Knockout of CYRI-B in myeloid cells results in a gain-of-function with regard to CEACAM3-mediated phagocytosis. (A) Schematic representation of the CYRI-B gene. A CRISPR/Cas9 gRNA was designed to target a region downstream of the ATG start codon (blue). The PAM sequence 3′ to the sgRNA target site is indicated in bold (*). To allow re-expression of CYRI-B in subsequent experiments, a CRISPR-Cas9 resistant CYRI-B cDNA was generated by introducing a total of five silent mutations in the gRNA target sequence and in the PAM sequence (indicated in red). (B) CYRI-B-deficient cell lines were established by transducing HL60 CEACAM3–mKate cells with a lentivirus encoding Cas9 and a sgRNA targeting CYRI-B as in A. Cells were selected with puromycin for 5 days and serially diluted to obtain clonal lines. Three CYRI-B deficient lines were established (C3, C6 and C7) as they did not express any detectable CYRI-B as determined by western blotting. In clone C4, CYRI-B expression was still detectable, albeit strongly reduced. Clone C6 was used as the CYRI-B-deficient cell line (CYRI-B ko) in subsequent experiments. Image representative of three experiments. (C) HL60 CEACAM3–mKate and CYRI-B ko cells were infected with CFSE- and biotin-labeled Ngo Opa_{52} or Ngo Opa^{-} for 15 min at an MOI of 30. Cells were fixed and extracellular bacteria were counter-stained with streptavidin–Alexa-Fluor-647 before samples were analyzed by confocal microscopy. Extracellular bacteria (arrowheads) are labeled with CFSE and Alexa-Fluor-647, whereas internalized bacteria show CFSE fluorescence only (arrows). Scale bar: 10 µm. (D) The number of intracellular Ngo Opa_{52} per cell was enumerated for the HL60 CEACAM3–mKate and the CYRI-B ko cells and is depicted in the bar graph (mean±s.d.; unpaired two-tailed Student's *t*-test, **P*<0.05; *n*=25 cells). (E,F) Internalization of CFSE-labeled Ngo-Opa_{52} or Ngo-Opa^{-} (E) and IgG-opsonized or non-opsonized Ngo-Opa^{-} (F) by HL60 CEACAM3–mKate and CYRI-B ko cells was evaluated by flow cytometry. Cells were infected for 15 min at a MOI of 30. Bars depict the mean CFSE fluorescence derived from intracellular bacteria normalized against CFSE fluorescence observed in HL60 CEACAM3–mKate cells infected with Ngo Opa_{52} (100%). Data are from three independent experiments (mean±s.d.; one-way ANOVA followed by a Dunnett's post test, **P*<0.05, ***P*<0.01; *n*=3).

(Fig. 3E). Again, non-opaque gonococci were hardly found inside the cells, whereas Opa_{52}-expressing bacteria were taken up by HL60 CEACAM3 cells and were internalized in even greater numbers by HL60 CEACAM3 CYRI-B ko cells (Fig. 3E). To investigate whether the lack of CYRI-B also affects opsonin-dependent phagocytic uptake, besides the opsonin-independent clearance via CEACAM3, we tested Fc-receptor-mediated phagocytosis by wild-type and CYRI-B ko HL60 cells. To this end, non-opaque gonococci were opsonized with rabbit anti-*N.gonorrhoeae* antibodies prior to infection. The non-opaque IgG-opsonized bacteria were readily internalized by HL60 CEACAM3 cells (Fig. 3F). Importantly, HL60 CEACAM3 CYRI-B ko cells showed a significantly increased uptake of the opsonized microbes, reflecting more than a doubling of bacterial internalization compared to that for the HL60 CEACAM3 cells (Fig. 3F). The uptake of these non-opaque bacteria was clearly mediated by Fc-receptors, as non-opsonized non-opaque gonococci were not internalized (Fig. 3F). These results indicate that lack of CYRI-B can enhance uptake by multiple phagocytic receptors, whereas receptor-independent engulfment of non-opsonized non-opaque gonococci, which neither engage with CEACAM3 nor Fc-receptors, is not affected (Fig. 3F).

CYRI-B deficiency results in elevated CEACAM3 signaling downstream of Rac

We wondered about the consequences of CYRI-B deficiency for Rac-dependent processes in phagocytes. Indeed, Rac activation in response to CEACAM3 engagement has been shown to direct the cytoskeletal rearrangements required for lamellipodia formation and efficient engulfment of particles (Schmitter et al., 2004; Schmitter et al., 2007). In line with a role of CYRI-B in dampening Rac signaling, CYRI-B ko cells showed elevated levels of GTP-bound Rac even in the absence of bacterial infection (Fig. 4A). As a consequence of the elevated Rac-GTP loading, downstream effectors of Rac, such as the p21-activated kinases PAK1 and PAK2 (hereafter collectively referred to as PAK) showed increased phosphorylation in HL60 CEACAM3 CYRI-B ko cells (Fig. 4B). PAK kinases have been implied in regulating F-actin dynamics via modulating LIM-kinase activity (Edwards et al., 1999), phosphorylation of Arp2/3 complex subunits (Vadlamudi et al., 2004) and inhibition of the guanine nucleotide exchange factor β-PIX (also known as ARHGEF7) (Davidson et al., 2021) suggesting that enhanced PAK activity could contribute to the phenotype of HL60 CEACAM3 CYRI-B ko cells. Accordingly, we used pharmacological inhibition of PAK with IPA-3 to interfere with PAK-dependent cytoskeletal dynamics. Indeed, pharmacological inhibition of PAK with IPA-3 severely diminished internalization of Opa_{52}-expressing *N. gonorrhoeae* by HL60 CEACAM3 and the HL60 CEACAM3 CYRI-B ko cells, suggesting that PAK is an important effector downstream of Rac-GTP (Fig. 4C). Moreover, de-regulated Rac activity in CYRI-B-deficient HL60 cells was accompanied by elevated F-actin levels (Fig. 4D). These findings imply that the enhanced Rac activity resulting from CYRI-B deficiency is responsible for the gain-of-function phenotype of CEACAM3-expressing phagocytes.

Complementation of HL60 CEACAM3 CYRI-B knockout cells reverts the phenotype

To verify that the phenotypes observed in CYRI-B-deficient cells are a direct consequence of the lack of this protein, we re-established CYRI-B expression in HL60 CEACAM3 CYRI-B ko cells. First, we introduced silent mutations in the sgRNA target sequence of the human CYRI-B cDNA (Fig. 3A). The resulting sgRNA-resistant version of CYRI-B wild-type (CYRI-B WT), fused to mCherry via a self-cleavable 2A peptide, was then stably re-introduced into HL60 CEACAM3 CYRI-B ko cells (Fig. 5A). Whole-cell lysates prepared from HL60 CEACAM3 CYRI-B ko CYRI-B wild-type (WT) re-expressing cells showed a ∼63 kDa band corresponding to the mCherry–CYRI-B fusion protein and a band at ∼37 kDa co-migrating with the endogenous CYRI-B observed in HL60 CEACAM3 cells (Fig. 5A). This is in line with previous reports indicating various degrees of self-cleaving activity by viral 2A peptides (Kim et al., 2011). Importantly, when these cells were infected with CFSE-labeled Opa_{52}-expressing *N. gonorrhoeae*, the elevated phagocytosis seen for the CYRI-B ko cells was strongly reduced, clearly demonstrating that the gain-of-function phenotype was indeed resulting from the lack of CYRI-B expression (Fig. 5B). Furthermore, although PAK phosphorylation was increased in HL60 CEACAM3 cells upon infection with Opa_{52}-expressing gonococci and PAK phosphorylation was even further elevated in HL60 CEACAM3 CYRI-B ko cells, the re-expression of CYRI-B in the CYRI-B ko cells suppressed the exaggerated PAK phosphorylation (Fig. 5C,D). In line with the increased levels of GTP-loaded Rac and phosphorylated PAK, HL60 CEACAM3 CYRI-B ko cells showed spontaneous formation of large lamellipodia when observed by scanning electron microscopy (Fig. 5E). Again, this gain-of-function phenotype was suppressed upon re-introduction of CYRI-B WT (Fig. 5E). These results clearly demonstrate that the intensified Rac-driven cytoskeletal processes in the HL60 CEACAM3 CYRI-B ko cells are a direct consequence of CYRI-B deficiency.

Journal of Cell Science (2023) 136, jcs260771. doi:10.1242/jcs.260771

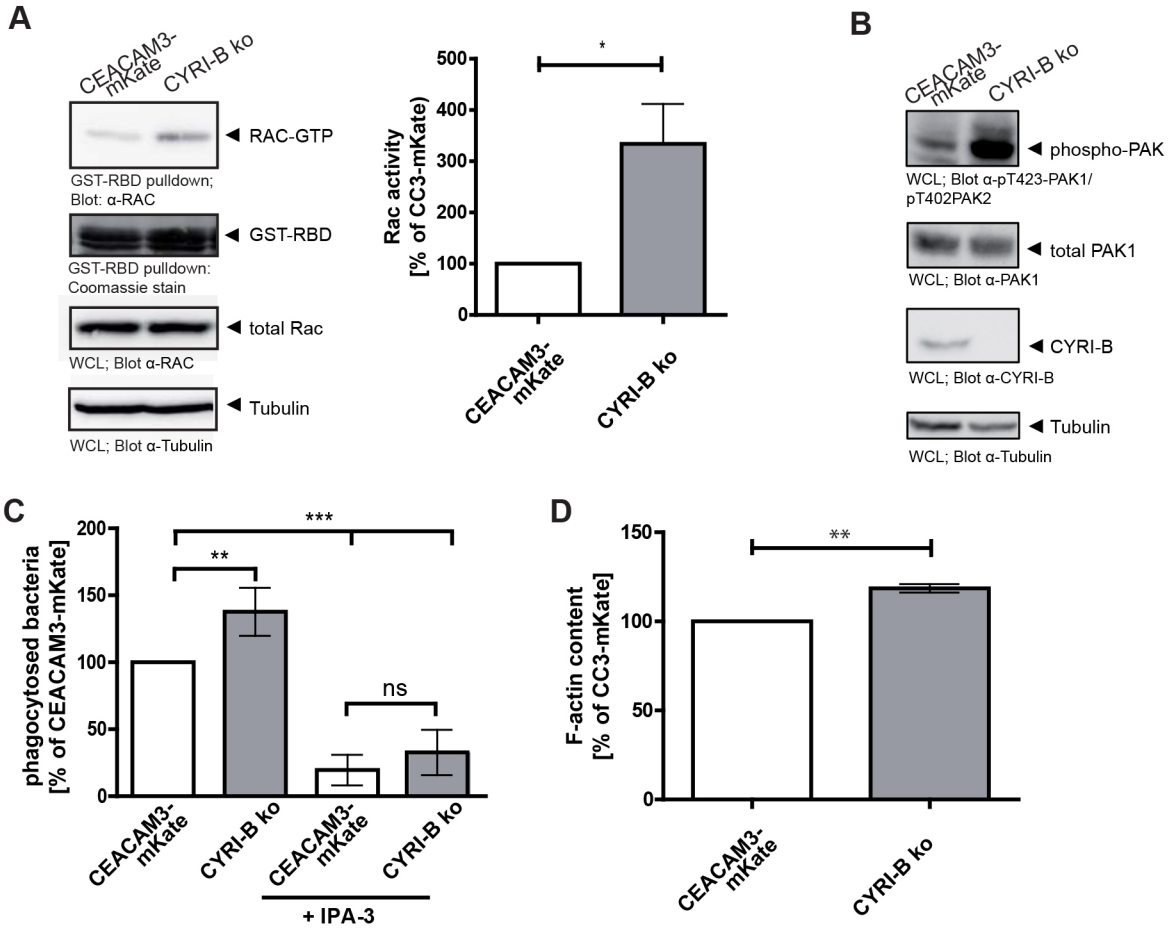

Fig. 4. CYRI-B deficiency results in elevated CEACAM3 signaling downstream of Rac. (A) Rac activity was measured in CC3-mKate and CYRI-B ko cells by GST-PAK-PBD pulldown assays (upper panels). Total Rac and tubulin are shown in the lower panels. Samples in lanes 3 and 4 were from cells infected with Ngo Opa_{52} at an MOI of 30 for 15 min. The bar diagram depicts the results of three independent experiments (mean±s.d.; unpaired two-tailed Student's *t*-test, **P*<0.05; *n*=3). (B) Cell extracts from CC3-mKate and CYRI-B ko cells were subjected to western blotting and expression of phospho-PAK1/2, total PAK1, CYRI-B and tubulin were analyzed. Image representative of three experiments. (C) CC3-mKate and CYRI-B ko cells were pre-treated with the PAK inhibitor IPA-3 or vehicle (10 µM, 30 min). Phagocytic activity was subsequently quantified by gentamycin protection assays and expressed as a percentage of that for CC3-mKate cells (mean±s.d.; one-way ANOVA followed by a Dunnett's post test, ***P*<0.01, ****P*<0.001; ns, not significant; *n*=4 independent experiments). (D) F-actin content of CC3–mKate and CYRI-B ko cells was quantified by FACS and expressed as a percentage of that for CC3-mKate (mean±s.d.; unpaired two-tailed *t*-test, ***P*<0.01; *n*=3).

CYRI-B-mediated sequestration of Rac GTP dampens PAK phosphorylation and phagocytosis

The CYRI-B-deficient HL60 CEACAM3 cells also afforded the possibility to investigate which functional domains are critical for the negative regulatory role of CYRI-B. To this end, we generated missense mutations in the sgRNA-resistant CYRI-B cDNA to disrupt the N-terminal myristoylation signal (CYRI-B G2A), to compromise the Rac-GTP binding interface (CYRI-B R160D/R161D) or a combination of both (CYRI-B G2A R160D/R161D) (Fig. 6A). These constructs or the mCherry-encoding empty virus were then introduced into the HL60 CEACAM3 CYRI-B ko cells and stable clonal cell lines were selected. Clones that re-expressed similar levels of the different CYRI-B variants were selected (Fig. 6B). Importantly, when these cells were infected with CEACAM-binding gonococci, re-expression of CYRI-B WT, but not introduction of mCherry, reduced the elevated internalization of bacteria back to the levels observed in HL60 CEACAM3 cells (Fig. 6C). The successful complementation of the HL60 CEACAM3 CYRI-B ko cells by the re-expression of WT CYRI-B confirmed the previous analysis and demonstrated that the gain-of-function phenotype of the CYRI-B-knockout cells is not based on an off-target effect of the CRISPR/Cas9 treatment. Moreover, expression of the Rac-binding-deficient CYRI-B R160D/R161D mutant was not able to revert the phenotype of the HL60 CEACAM3 CYRI-B ko cells, demonstrating that the effect of CYRI-B on CEACAM3-mediated phagocytosis depends on its ability to sequester GTP-bound Rac (Fig. 6C). In contrast, the myristoylation of CYRI-B was not required, as CYRI-B G2A was perfectly fine in diminishing the exaggerated phagocytosis of CEACAM3-binding gonococci (Fig. 6C). Importantly, these functional data with regard to phagocytosis were mirrored by the PAK phosphorylation levels in the different cell lines (Fig. 6D). Re-expression of CYRI-B WT and CYRI-B G2A reduced the elevated PAK phosphorylation levels back to background levels, whereas re-expression of mCherry alone, CYRI-B–mCherry R160D/R161D, or CYRI-B-mCherry G2A R160D/R161D did not revert the phenotype (Fig. 6D). Together, these findings demonstrate that CYRI-B limits CEACAM3-initiated responses by sequestering the small GTPase Rac, thereby controlling the extent of CEACAM3-driven downstream processes.

Journal of Cell Science (2023) 136, jcs260771. doi:10.1242/jcs.260771

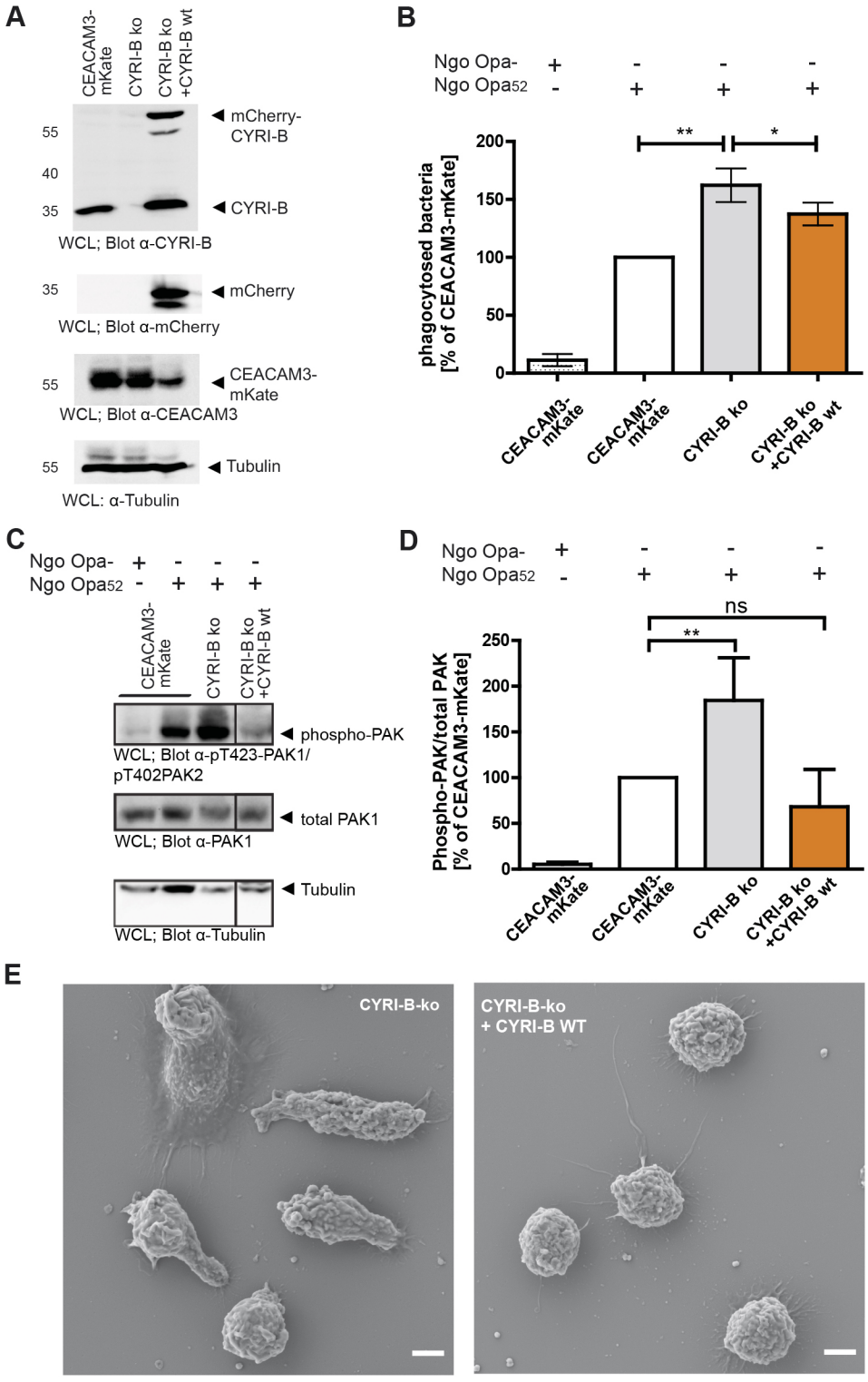

Fig. 5. Complementation of HL60 CEACAM3 CYRI-B knockout cells reverts the phenotype. (A) CYRI-B ko cells were transduced with a lentiviral construct encoding a sgRNA-resistant version of CYRI-B wt. Whole-cell lysates (WCLs) of these cells were analyzed by western blotting together with WCLs from HL60 CEACAM3–mKate and CYRI-B ko cells. Membrane was probed with antibodies against CYRI-B (upper panel), mCherry (second panel), CEACAM3 (third panel) or tubulin (lower panel). Image representative of two experiments. (B) CEACAM3-mediated phagocytosis was determined by flow cytometry. The indicated cell lines were infected with CFSE-labeled non-opaque (Ngo Opa^{-}) or Opa$_{52}$-expressing *N. gonorrhoeae* (Ngo Opa$_{52}$) for 15 min at a MOI of 30. Bars depict the mean phagocytotic activity normalized against CEACAM-mKate from three independent experiments (mean±s.d.; one-way ANOVA followed by a Dunnett's post test, **P*<0.05, ***P*<0.01; *n*=3). (C) PAK phosphorylation was assessed by western blotting in WCLs of indicated cell lines infected as in B. Samples were probed with polyclonal antibodies against phosphoT423-PAK1 and phosphoT402-PAK2 (phospho-PAK, upper panel), polyclonal antibodies against total PAK1 (middle panel) or a monoclonal antibody against tubulin (lower panel). (D) The experiment in (C) was repeated and signals were quantified by densitometry. Bars represent ratios of phospho-PAK1/PAK2 versus total PAK1 normalized to Ngo Opa$_{52}$-infected HL60 CEACAM3–mKate cells. Data are from three independent experiments (mean±s.d.; one-way ANOVA followed by a Dunnett's post test; ns, not significant, ***P*<0.01; *n*=3). (E) Scanning electron microscopy images of CYRI-B ko (left panel) and CYRI-B ko cells re-expressing CYRI-B wt (right panel) infected with Ngo Opa$_{52}$. Images representative of three experiments. Scale bars: 5 µm.

DISCUSSION

CEACAM3 is a specialized phagocytic receptor, enabling primate granulocytes to recognize and eliminate a restricted set of host-adapted bacterial pathogens (Bonsignore et al., 2019). To detect novel cellular regulators of CEACAM3-mediated phagocytosis, we performed an unbiased, genome-wide genetic screen in a human myeloid cell line. Although loss-of-function effects were seen for several genes, including components of the cytoskeleton, we focused our attention on genes whose disruption consistently resulted in a gain-of-function with regard to the uptake of CEACAM3-engaging microbes. We predicted that such a phenotype should arise from the deletion of factors with a negative regulatory role in CEACAM3-mediated phagocytosis.

In agreement with this prediction, abrogating the expression of the CYFIP-related Rac interactor B (CYRI-B), one of the factors

Journal of Cell Science (2023) 136, jcs260771. doi:10.1242/jcs.260771

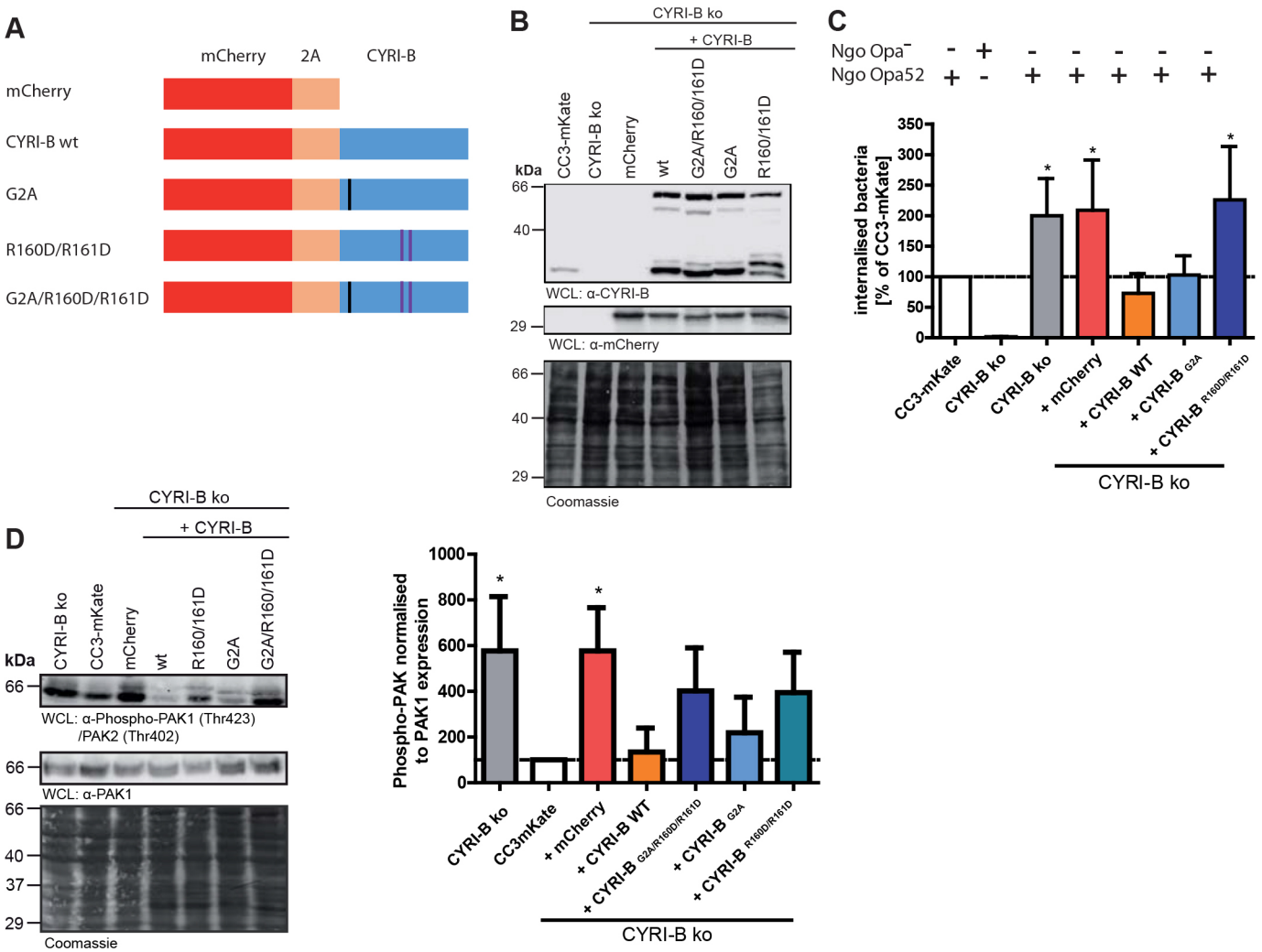

Fig. 6. CYRI-B-mediated sequestration of Rac GTP dampens PAK phosphorylation and phagocytosis. (A) Schematic outline of the missense mutations introduced into the sgRNA-resistant mCherry-CYRI-B WT fusion construct resulting in mCherry–CYRI-B-G2A, mCherry–CYRI-B-R160D/R161D, mCherry-CYRI-B-R-G2A/R160D/R161D or mCherry alone. (B) CYRI-B ko cells were transduced with lentiviral constructs from (A). Whole-cell lysates (WCLs) were analyzed by western blotting with antibodies against CYRI-B (upper panel), against mCherry (middle panel) or against tubulin (lower panel). (C) CEACAM3-mediated phagocytosis of Ngo Opa_{52} or non-opaque gonococci (Ngo Opa^{-}) by the complemented cell lines from B was quantified using gentamicin protection assays. The number of recovered bacterial colonies was determined and normalized against the uptake of Ngo Opa52 bacteria by HL60 CEACAM3–mKate cells. Bars represent mean±s.d. of five independent experiments (one-way ANOVA followed by a Dunnett's post test, **P*<0.05; *n*=5). (D) WCLs from cells as in B were analyzed by western blotting with rabbit polyclonal antibodies against phoshoT423-PAK1/phosphoT402-PAK2 (upper panel), polyclonal antibodies against total PAK1 (middle panel), or the membrane was stained with Coomassie to reveal the total loaded protein (lower panel). (E) The experiment in D was repeated and signals were quantified by densitometry. Bars represent ratios of phosphoPAK1/PAK2 versus total PAK1 normalized to HL60 CEACAM3-mKate cells. Data are from four independent experiments (mean±s.d.; one-way ANOVA followed by a Dunnett's post test, **P*<0.05; *n*=4).

identified in the screen, led to elevated internalization of CEACAM-binding *Neisseria gonorrhoeae*. Owing to the Rac-GTP sequestering activity of CYRI-B, it has been previously observed that CYRI-B diminishes Rac-GTP-initiated downstream signaling and thereby interferes with Rac-dependent actin dynamics (Fort et al., 2018; Shang et al., 2018). This function of CYRI-B can directly explain the phenotype with regard to CEACAM3-mediated phagocytosis observed for the CYRI-B-deficient cells. Indeed, compromising the Rac-binding interface of CYRI-B at residues R160 and R161 also abrogates the effect of CYRI-B on CEACAM3. The recent crystal structure (PDB: 7AJK) of CYRI-B in complex with Rac nicely reveals why CYRI-B selectively acts on Rac, but not on other related Rho family GTPases, such as Cdc42 (Yelland et al., 2021). Therefore, the surfacing of CYRI-B as a negative regulator of CEACAM3-mediated phagocytosis in this unbiased screening approach highlights the central role played by Rac in CEACAM3-initiated cellular responses. Although earlier studies employing CEACAM3-expressing HeLa cells indicated a contribution of the Rho family GTPase Cdc42 for CEACAM3-dependent bacterial internalization (Billker et al., 2002), investigations in myeloid cell lines and primary human granulocytes pointed to a specific and exclusive function of Rac, but not Cdc42, downstream of CEACAM3 (Hauck et al., 1998; Schmitter et al., 2004). This tight connection between CEACAM3 and Rac is not only further emphasized by the involvement of the WAVE/Scar complex in regulating the cytoskeletal rearrangements necessary for CEACAM3-driven phagocytosis (Pils et al., 2012), but is now underscored by our finding of a prominent

negative-regulatory role of CYRI-B. In this respect, CYRI-B structurally mimics the CYFIP component of the WAVE complex, functioning as a competitive inhibitor of Rac-GTP-dependent stimulation of Scar/WAVE and its Arp2/3-complex-mediated actin nucleating activity (Yelland et al., 2021; Kaplan et al., 2020). In line with the idea that Rac is the critical Rho family GTPase in CEACAM3-initiated phagocytosis, our screen not only uncovers, with CYRI-B, a selective negative regulator of Rac, but also indicates that the Rac-specific guanine nucleotide exchange factor Dock3 could play a positive role in this process.

Exaggerated activation of Rac can lead to massive cytoskeletal re-organization and, via the activation of the NADPH oxidase, to the production of reactive oxygen species. Therefore, this process needs to be constrained in its magnitude, but also needs to be spatially confined to maximize the formation of productive lamellipodial protrusions. Accordingly, CYRI-B could provide local and/or temporal regulation of Rac to prevent excessive phagocyte responses during infection, which could damage host tissues. Recently, CYRI-B has also been shown to protect animals from infections by facultative intracellular pathogens, such as *Salmonella*, *Mycobacterium* and *Listeria*, which enter and multiply in phagocytes (Yuki et al., 2019). In this scenario, the reduction in phagocytosis afforded by CYRI-B seems to reduce the chances of these microbes for intracellular multiplication and systemic spread via macrophages (Yuki et al., 2019).

How CYRI-B itself is regulated, is currently unclear. Based on the crystal structure, Yelland et al. have suggested the existence of an autoinhibited CYRI-B dimer, which is not able to bind the small GTPase (Yelland et al., 2021). By a rachet-like movement of a C-terminal α-helical bundle, CYRI-B would need to first attain the proper conformation for associating with Rac-GTP (Yelland et al., 2021). Accordingly, binding interactions or post-translational modifications of the CYRI-B C-terminal portion might trigger the resolution of the CYRI-B dimer and allow CYRI-B binding to Rac-GTP. Indeed, several lysine residues in the C-terminus of CYRI-B are the target of ubiquitylation (Uniprot entry Q9NUQ9; https://www.phosphosite.org/proteinAction.action?id=19888&showAllSites=true), a modification, which could guide the large conformational changes in CYRI-B. Interestingly, our screen for modulators of CEACAM3-mediated phagocytosis also identified enzymes involved in mono- or poly-ubiquitylation such as TRIM61. Although their actual contribution is currently unclear, it will be interesting to unravel a potential functional connection between such enzymes and CYRI-B modifications in CEACAM3-mediated phagocytosis.

In conclusion, a genome-wide genetic screen to unravel factors influencing CEACAM3-mediated phagocytosis has not been conducted previously. The screening results could be verified by identifying CYRI-B as a negative regulator of CEACAM3-initiated processes and yielded additional leads for further investigation. Our results, therefore, provide an initial framework to comprehensively describe the processes and individual proteins that orchestrate this innate immune defense.

MATERIALS AND METHODS

Antibodies

The following primary and secondary antibodies were used. Primary antibodies were against the following proteins: CEACAM3/CEA [mouse monoclonal, clone 308/3-3 from ImmunoTools, Friesoythe, Germany; western blotting (WB): 1:2000, flow cytometry (FC): 1:200]; GFP (mouse monoclonal, clone JL8, lot A5033481 from Clontech, Mountain View, CA, WB: 1:5000); RFP (used to detect mCherry, mouse monoclonal, clone 6G6, lot 51020014AB-01 from Chromo Tek, Martinsried, Germany, WB: 1:2000); tubulin (mouse monoclonal, clone E7 from Developmental Studies Hybridoma Bank, University of Iowa, IA, WB: 1:1000); Rac (mouse monoclonal #PA5-17519 from Thermo Fisher Scientific, WB: 1:1000); CYRI-B (mouse monoclonal, clone D8, lot H2817, from Santa Cruz Biotechnology, WB: 1:500); phospho-PAK1-(Thr423)/phospho-PAK2-(Thr402) (rabbit polyclonal #2601, lot 18 from Cell Signaling Technology, WB: 1:1000); PAK1 (rabbit polyclonal #2602 from Cell Signaling Technology, WB: 1:1000); anti-*N. gonorrhoeae*/anti-*N.meningitidis* (rabbit polyclonal; IG-511, custom made by Immunoglobe, Himmelstadt, Germany; Kuespert et al., 2011). Secondary antibodies were horseradish peroxidase (HRP)-conjugated goat anti-mouse-IgG (WB: 1:10,000) and HRP-conjugated goat anti-rabbit-IgG (WB: 1:5000) were from Jackson ImmunoResearch (Baltimore, MD).

Recombinant DNA

The plasmid pLL3.7 encoding a CMV-promoter driven expression cassette of GFP was Addgene plasmid #11795, deposited by Luk Parijs (Rubinson et al., 2003). The plasmid plentiCRISPR v2 sgRNA-Cerulean containing a Cerulean targeting sgRNA has been described previously (Grimm et al., 2020). Human GeCKOv2 CRISPR knockout pooled library was Addgene plasmid #1000000048 (deposited by Feng Zhang) and the A part of the pooled library was used in the screen (Sanjana et al., 2014). The CYRI-B-targeting plasmid pLentiCRISPRv2-sgCYRI-B was generated by digesting pLentiCRISPRv2 (Addgene plasmid #52961, deposited by from Feng Zhang) with BsmBI and insertion of a CYRI-B targeting oligonucleotide (using the annealed sense oligonucleotide 5′-CACCGGACATGCACA-GACCTTGAGC-3′ and antisense oligonucleotide 5′-AAACGCTCAA-GGTCTGTGCATGTCC-3′).

To re-express CYRI-B in CYRI-B ko cells the CYRI-B ORF was amplified by PCR from HsCD00369072 (PlasmID, Harvard Medical School repository) with primers (forward, 5’-ACTCCTCCCCCGC-CATGGGGAATCTTCTTAAAGTTTTGAC-3′ and reverse, 5’-CCCCAC-TAACCCGTTGCAGCATGGATTTAATTTGC-3′) containing sequences compatible with ligase independent cloning (LIC) into the vector pDNR-Dual-LIC (Adrian et al., 2019). To render CYRI-B insensitive to the CRISPR gRNA used to create the knockout cell line, site-directed mutagenesis was performed with overlapping primers (forward, 5′-CTTCTTAAAGTTTTGACCTGTACCGATTTGGAACAGGGGCCAAA-TTTTTTCC-3′ and reverse, 5′-GGAAAAAATTTGGCCCCTGTTC-CAAATCGGTACAGGTCAAAACTTTAAGAAG-3′). The resulting construct contains five silent mutations in the CRISPR gRNA-binding region in CYRI-B. This Cas9-insensitive mutant (CYRI-wt) was used as a template for site-directed mutagenesis to create the G2A mutant (forward, 5′-CTCCTCCCCCGCCATGGCCAATCTTCTTAAAGTTTTG-3′ and reverse, 5′-CAAAACTTTAAGAAGATTGGCCATGGCGGGGGAGGAG-3′) and the R160D/R161D mutant (forward, 5′-GAATGATTTCAGCTATTATGAT-GACACATTGAGTCGTATGAGG-3′ and reverse, 5’-CCTCATACGACT-CAATGTGTCATCATAATAGCTGAAATCATTC-3′). To transfer the Cas9-resistant versions of CYRI-B WT and R160D/R161D into a lentiviral expression vector, the ORFs were amplified by PCR (forward, 5′-GATACCCGGGATGGGGAATCTTCTTAAAGTTTTGAC-3′ and reverse, 5’-GAGTGAATTCTCATTGCAGCATGGATTTAATTTGC-3′) as were CYRI-G2A and CYRI-G2A/R160D/R161D (Forward, 5′-GAATCCCGG-GATGGCCAATCTTCTTAAAGTTTTGAC and reverse: 5’-GAGTGAA-TTCTCATTGCAGCATGGATTTAATTTGC-3′) using primers with SmaI and EcoRI restriction sites. The PCR products were ligated in SmaI and EcoRI of the lentiviral vector pUltra-Hot (Addgene plasmid #24130, deposited by Malcolm Moore).

Cell culture

HL60 cells (CCL-240, ATCC, Manassas, Virginia) and the derived HL60 CEACAM3 mKate cells (Adrian et al., 2019) were cultured in RPMI 1640 medium (Gennaxxon, C4095) supplemented with 10% fetal calf serum (FCS; Gibco, 10279-106, lot no. 2166469), maintained at 37°C and 5% CO_2 and were split every 2–3 days. HL60 Cerulean cells were generated by lentiviral transduction of HL60 cells with a Cerulean-encoding lentivirus (Goob et al., 2022). At 5 days after transduction, single Cerulean-positive cells were sorted on a FACS AriaIII (BD Biosciences)

into 96-well plates and a single-cell-derived HL60 Cerulean clone was expanded.

Human embryonic kidney 293 T cells (293 T; American Type Culture Collection CRL-3216) were grown in DMEM (Gennaxon, C4036) supplemented with 10% calf serum (Biowest, S0750, batch S00O510006). For transient transfection, 293 T cells were seeded at 25% confluence the day before and transfected using calcium phosphate precipitation.

The cell lines were regularly tested by PCR according to Uphoff and Drexler (2005) for the presence of mycoplasma contamination and confirmed to be negative. They were not further authenticated.

Lentivirus production in 293 T cells and transduction of HL60 cells

Lentiviral particles were produced by transient transfection of 293 T cells with the plasmids pMD2.G (Addgene #12259) (3.5 µg), psPAX2 (Addgene #12260) (5 µg), and the respective lentiviral vector (6.5 µg). At 3 days after transfection, the virus-containing supernatant was collected, sterile filtered (pore size 0.45 µm) and added to the recipient cells, which also received 8 µg/ml hexadimethrine bromide. Virus-infected HL60 cells were centrifuged at 800 ***g*** for 1 h to spin the viral particles onto the cells (spinfection). pLentiCRISPRv2 transduced cells were selected with 0.3 µg/ml puromycin for 5 days before bacterial uptake and sorting by FACS.

Immunofluorescence staining of HL60 cells for flow cytometry

10^6 cells were taken up in FACS buffer (PBS, 5% FCS) and transferred to Eppendorf tubes. Cells were centrifuged at 650 ***g*** for 2 min at 4°C and incubated with the primary antibody in FACS buffer for 1 h on ice. Samples were washed three times with FACS buffer and then incubated with the fluorescently labeled secondary antibody in FACS buffer for 30 min at 4°C in the dark. Cells were washed as before, suspended in 600 µl FACS buffer, and transferred to FACS tubes. Finally, cells were analyzed by flow cytometry (BD LSRII, FACSDiva software; BD Biosciences) and obtained data were evaluated using the FlowJo software package.

Whole-cell lysates and western blotting

Cells were lysed in RIPA buffer (0.1% w/v SDS, 1% sodium deoxycholic acid, 1% Triton X-100, 50 mM Hepes, 150 mM NaCl, 10% glycerol, 1.5 mM $MgCl_2$, 1 mM EGTA, 10 mM sodium pyrophosphate and 100 mM NaF) or NP40 lysis buffer (50 mM Tris-HCl, pH 7.4, 150 mM NaCl, 1% NP40, 1 mM EDTA, 50 mM NaF) in the presence of protease inhibitors (aprotinin from Roth, Karlsruhe, Germany, and leupeptin and PMSF from Applichem, Darmstadt, Germany), 1 mM sodium orthovanadate and 10 mM of para-nitrophenol phosphate. After centrifugation at 18,000 ***g*** and 4°C for 30 min, cleared whole-cell lysates were taken up in SDS buffer and boiled at 95°C for 5–10 min. Proteins were separated by SDS-PAGE and transferred to PVDF membranes. Subsequently, membranes were blocked in blocking buffer (50 mM Tris-HCl pH 7.5, 150 mM NaCl, 0.05% Tween 20 and 2% BSA) for 1 h at room temperature (RT) and then incubated with primary antibodies (diluted in blocking buffer) overnight at 4°C. The next day, membranes were washed three times with TBS-T (50 mM Tris-HCl pH 7.5, 150 mM NaCl and 0.05% Tween 20) and incubated with the HRP-conjugated secondary antibody (in TBS-T) for 1 h at RT, before ECL detection on a Chemidoc Touch Imaging System (Bio-Rad, CA). Full-size scans of all western blots used to generate the cropped panels depicted in the main figures are compiled in Fig. S3.

Bacterial strains and growth conditions

N. gonorrhoeae MS11-B2.1 strains (non-piliated Opa_{52}-expressing strain N309 and non-piliated, non-opaque strain N302) (Kupsch et al., 1993) were grown on GC agar plates supplemented with vitamins. Bacteria were cultured at 37°C and 5% CO_2 and freshly streaked on plates 16–20 h before experiments.

Analysis of bacterial uptake by flow cytometry

10^6 CEACAM3–mKate2-expressing HL60 cells were suspended in 1 ml phagocytosis buffer (PBS, 0.9 mM $CaCl_2$, 0.5 mM $MgCl_2$, 5 mM glucose, 1% heat-inactivated FCS). Opa_{52}-expressing *N. gonorrhoeae* (Ngo Opa_{52}) or non-opaque gonococci (Ngo Opa-) were re-suspended in 1 ml PBS, stained by addition of 2 µg/ml 5/6-carboxyfluorescein succinimidyl ester (CFSE; Molecular Probes, Karlsruhe, Germany) for 20 min with constant shaking in the dark, and then washed three times with PBS (4 min, 1700 ***g***). For opsonization with IgG, CFSE-stained Ngo Opa^- were incubated 30 min at 37°C with 20% heat-inactivated rabbit anti-*N.gonorrhoeae* serum (IG-511) and subsequently washed two times with PBS. Cells were infected for the indicated time at the indicated MOI under gentle rotation at 37°C. To stop bacterial uptake, samples were washed with ice-cold PBS, taken up in ice-cold phagocytosis buffer and mixed with Trypan Blue (final concentration 0.2 mg/ml) to quench the CFSE signal derived from extracellular bacteria (Pils et al., 2006). Bacterial uptake was analyzed by flow cytometry using a FACS Fortessa (BD Biosciences), and raw data were analyzed using FlowJo software.

Analysis of bacterial uptake by FBA staining

To discriminate between extracellular and internalized bacteria, FITC–biotin–avidin staining was employed as described (Agerer et al., 2004). To this end, HL60 cells were seeded onto poly-L-lysine-coated coverslips and allowed to adhere overnight in RPMI with 1% FCS. Opa_{52}-expressing *N. gonorrhoeae* were washed with PBS, stained with 2 µg/ml 5/6-carboxyfluorescein succinimidyl ester (CFSE; Molecular Probes, Karlsruhe, Germany) and simultaneously surface biotinylated with Sulfo-NHS–LC–biotin (Perbio Science, Bonn, Germany). After washing the bacteria three times with PBS, the labeled bacteria were used to infect the adherent cells for 15 min at a MOI 30. Infected samples were washed with cold PBS and fixed with 4% PFA in PBS for 20 min and washed three times with PBS. Extracellular bacteria were counter-stained with streptavidin–Alexa-Fluor-647 (10 µg/ml, Molecular Probes, S3235) for 1 h at RT in the dark. Samples were washed three times with PBS and mounted on glass slides using Dako Mounting Medium (Dako). Finally, samples were imaged using a Leica SP5 confocal microscope to detect intracellular bacteria (CFSE staining only) and extracellular bacteria (CFSE and Alexa-Fluor-647 staining).

Amplicon sequencing

Genomic DNA was isolated from the input cell population and sorted cell populations with a genomic DNA isolation kit (PureLink) and used as template (125 ng per reaction) in multiple PCRs (Phusion polymerase, HF buffer, Thermo Fisher Scientific) using primers flanking the sgRNA sequences (forward primer 5′-CTTGAAAGTATTTCGATTTCTTGGC-3′ and reverse primer 5′-CCTTTCAAGACCTAGCTAGCG-3′). After initial denaturation (90 s, 98°C), 30 cycles of amplification were performed (25 s, 57°C; 7 s, 72°C; 10 s, 98°C). PCR products were isolated from an agarose gel (1.5%) and extracted using a gel extraction kit (Genaxxon). Eluates were sent for sequencing on an Illumina sequencing platform (2×150 PE, Eurofins). The sequencing data have been deposited at the NCBI Sequence Read Archive under the BioProject ID PRJNA957296, containing three separate Biosamples SAMN34249396 (input population), SAMN34249397 (low phagocytosis) and SAMN34249398 (high phagocytosis). Raw paired-end reads were merged using FLASH (Magoc and Salzberg, 2011). Read abundances per gene were determined in each sample and normalized for the total number of reads (normalized read abundance). Finally, the normalized read abundance in the 'low' and 'high' phagocytic samples were divided by the normalized read abundance of the 'input population' sample to obtain the enrichment ratio.

CEACAM pulldown from HL60 cell lysates

Opa_{52}-expressing *N. gonorrhoeae* were fixed in 4% paraformaldehyde-containing PBS for 20 min and then washed three times with PBS. Fixed bacteria were added to HL60 cell lysates and rotated at 4°C for 3 h. Bacteria-bound CEACAMs were precipitated at 2650 ***g*** for 5 min, washed twice with PBS, and boiled in 2× Laemmli loading buffer.

Gentamicin protection assay with HL60 cells

HL60 cells were seeded in triplicate into poly-L-lysine-coated 12-well plates at 3×10^5 cells/well in serum-free medium and infected for 15 min at an MOI of 30 with Opa_{52}-expressing *N. gonorrhoeae* (Opa_{52}) or *N. gonorrhoeae* that do not express Opa proteins (Opa^-). Extracellular bacteria were killed

by a 45-min incubation in culture medium containing 50 µg/ml gentamicin. Infected cells were lysed with 0.5% (w/v) saponin in PBS for 15 min, and released bacteria were plated on GC agar plates at various dilutions. The re-isolated colony forming unit (cfu) values were determined and statistical analysis of three independent experiments was performed using a one-way ANOVA followed by a Dunnett's post test.

Determination of Rac GTP loading

Rac activity was determined with a pulldown assay using the recombinant PAK p21-binding domain (PBD) fused to GST (Schmitter et al., 2004). For each pulldown, 1×10^7 HL60 cells were lysed (50 mM Tris, pH 7.5, 200 mM NaCl, 5 mM $MgCl_2$, 1 mM DTT, 10% glycerol, 1% NP40, 1 mM PMSF, 10 µg/ml aprotinin and 10 µg/ml leupeptin) on ice for 20 min and centrifuged for 10 min at 4°C at 20,000 ***g***. Supernatant containing equal amounts of protein were transferred to a new tube, input samples were taken and 25 µl Sepharose–PBD beads (10 µg GST–PBD) were added. After binding for 1 h at 4°C on a rotator (15 rpm). Beads were washed three times with PBD wash buffer (25 mM Tris-HCl pH 7.5, 40 mM NaCl, 30 mM $MgCl_2$, 1 mM DTT, 1%, 1 mM PMSF, 10 µg/ml aprotinin and 10 µg/ml leupeptin) and subsequently boiled in 2× Laemmli loading buffer. Input samples and PBD pulldown samples were run on the same SDS-PAGE gel followed by western blotting.

F-actin quantification

HL60 cells (0.5×10^6) were fixed in 4% PFA for 30 min at 37°C on a rotator (15 rpm), washed with PBS and subsequently permeablized for 3 min at RT (PBS with 0.1% TritonX-100 and 5% BSA). F-actin was stained with phalloidin-conjugated Alexa-Fluor-488 (Molecular Probes, 1:50 in PBS with 0.5% BSA) for 45 min at RT. Cells were washed twice with PBS and resuspended in FACS buffer. The mean fluorescence intensity (MFI) of 10,000 cells per sample was determined by FACS analysis.

Scanning electron microscopy

HL60 cells were seeded at 4×10^4 cells/well in phagocytosis buffer on 12 mm glass coverslips coated with poly-L-lysine (10 mg/ml). Cells were infected for 30 min with Opa_{52}-expressing *N. gonorrhoeae* at an MOI of 30. Samples were fixed at 4°C for a total of 60 min in EM fixative (0.1 M HEPES, pH 7.2, 3% formaldehyde, 2% glutaraldehyde, 0.09 M sucrose, 0.01 M $CaCl_2$ and 0.01 M $MgCl_2$) that was renewed one time. Fixed samples were washed three times with washing buffer (0.1 M HEPES, pH 7.2, 0.09 M sucrose, 0.01 M $CaCl_2$ and 0.01 M $MgCl_2$) and dehydrated in an ethanol gradient, critical point dried with liquid CO_2 (BAL-TEC SCD 030 Critical Point Dryer) and sputter-coated with 8 mm gold-palladium. Samples were imaged at 5 kV in a field emission scanning electron microscope (Auriga; Carl Zeiss AG, Jena, Germany).

Statistics

Data are presented as mean±s.d. as indicated in the figure legend. Statistical significance was determined with either an unpaired two-tailed Student's *t*-test or a one-way ANOVA followed by a Dunnett's post test, using Prism5 (GraphPad). The significance level was set at $P<0.05$ and is indicated by $*P<0.05$, $**P<0.01$, $***P<0.001$, or ns, not significant. Further statistical details are provided in the figures and figure legends.

Acknowledgements

We thank S. Feindler-Boeckh and C. Hentschel for expert technical assistance. We are grateful to the Flow Cytometry facility of the Department of Biology, Konstanz University (FlowKon) and Michael Laumann (Electron Microscopy Service of the Department of Biology, University of Konstanz) for support and sample analysis.

Competing interests

The authors declare no competing or financial interests.

Author contributions

Conceptualization: J.W.P.K., J.A., C.R.H.; Methodology: J.W.P.K., J.K., L.P., J.A., C.R.H.; Investigation: J.W.P.K., J.K., L.P., J.A.; Writing - original draft: C.R.H.; Writing - review & editing: J.W.P.K., C.R.H.; Supervision: C.R.H.; Funding acquisition: C.R.H.

Funding

This study was supported by funds from the Deutsche Forschungsgemeinschaft (Ha 2856/10-1; Ha 2856/11-1) to C.R.H. The funding body was not involved in the design, in the collection, analysis, and interpretation of data; in the writing of the manuscript; nor in the decision to submit the manuscript for publication.

Data availability

All primary data relevant to this study are included within this manuscript, except for the raw sequencing data, which have been deposited at the NCBI Sequence Read Archive under the BioProject ID PRJNA957296.

Peer review history

The peer review history is available online at https://journals.biologists.com/jcs/lookup/doi/10.1242/jcs.260771.reviewer-comments.pdf.

References

Adrian, J., Bonsignore, P., Hammer, S., Frickey, T. and Hauck, C. R. (2019). Adaptation to host-specific bacterial pathogens drives rapid evolution of a human innate immune receptor. *Curr. Biol.* **29**, 616-630.e5. doi:10.1016/j.cub.2019.01.058

Agerer, F., Waeckerle, S. and Hauck, C. R. (2004). Microscopic quantification of bacterial invasion by a novel antibody-independent staining method. *J. Microbiol. Methods* **59**, 23-32. doi:10.1016/j.mimet.2004.05.008

Beauchemin, N. and Arabzadeh, A. (2013). Carcinoembryonic antigen-related cell adhesion molecules (CEACAMs) in cancer progression and metastasis. *Cancer Metastasis Rev.* **32**, 643-671. doi:10.1007/s10555-013-9444-6

Billker, O., Popp, A., Brinkmann, V., Wenig, G., Schneider, J., Caron, E. and Meyer, T. F. (2002). Distinct mechanisms of internalization of *Neisseria gonorrhoeae* by members of the CEACAM receptor family involving Rac1- and Cdc42- dependent and -independent pathways. *EMBO J.* **21**, 560-571. doi:10.1093/emboj/21.4.560

Bonsignore, P., Kuiper, J. W. P., Adrian, J., Goob, G. and Hauck, C. R. (2019). CEACAM3-A Prim(at)e invention for opsonin-independent phagocytosis of bacteria. *Front. Immunol.* **10**, 3160. doi:10.3389/fimmu.2019.03160

Buntru, A., Kopp, K., Voges, M., Frank, R., Bachmann, V. and Hauck, C. R. (2011). Phosphatidylinositol-3' kinase activity is critical for initiating the oxidative burst and bacterial destruction during CEACAM3-mediated phagocytosis. *J. Biol. Chem.* **286**, 9555-9566. doi:10.1074/jbc.M110.216085

Buntru, A., Roth, A., Nyffenegger-Jann, N. J. and Hauck, C. R. (2012). HemITAM signaling by CEACAM3, a human granulocyte receptor recognizing bacterial pathogens. *Arch. Biochem. Biophys.* **524**, 77-83. doi:10.1016/j.abb.2012.03.020

Davidson, A., Tyler, J., Hume, P., Singh, V. and Koronakis, V. (2021). A kinase-independent function of PAK is crucial for pathogen-mediated actin remodelling. *PLoS Pathog.* **17**, e1009902. doi:10.1371/journal.ppat.1009902

Delgado Tascon, J., Adrian, J., Kopp, K., Scholz, P., Tschan, M. P., Kuespert, K. and Hauck, C. R. (2015). The granulocyte orphan receptor CEACAM4 is able to trigger phagocytosis of bacteria. *J. Leukoc. Biol.* **97**, 521-531. doi:10.1189/jlb.2AB0813-449RR

Edwards, D. C., Sanders, L. C., Bokoch, G. M. and Gill, G. N. (1999). Activation of LIM-kinase by Pak1 couples Rac/Cdc42 GTPase signalling to actin cytoskeletal dynamics. *Nat. Cell Biol.* **1**, 253-259. doi:10.1038/12963

Fort, L., Batista, J. M., Thomason, P. A., Spence, H. J., Whitelaw, J. A., Tweedy, L., Greaves, J., Martin, K. J., Anderson, K. I., Brown, P. et al. (2018). Fam49/CYRI interacts with Rac1 and locally suppresses protrusions. *Nat. Cell Biol.* **20**, 1159-1171. doi:10.1038/s41556-018-0198-9

Goob, G., Adrian, J., Cossu, C. and Hauck, C. R. (2022). Phagocytosis mediated by the human granulocyte receptor CEACAM3 is limited by the receptor-type protein tyrosine phosphatase PTPRJ. *J. Biol. Chem.* **298**, 102269. doi:10.1016/j.jbc.2022.102269

Goodridge, H. S., Underhill, D. M. and Touret, N. (2012). Mechanisms of Fc receptor and dectin-1 activation for phagocytosis. *Traffic* **13**, 1062-1071. doi:10.1111/j.1600-0854.2012.01382.x

Grimm, T. M., Dierdorf, N. I., Betz, K., Paone, C. and Hauck, C. R. (2020). PPM1F controls integrin activity via a conserved phospho-switch. *J. Cell Biol.* **219**, e202001057. doi:10.1083/jcb.202001057

Hauck, C. R., Meyer, T. F., Lang, F. and Gulbins, E. (1998). CD66-mediated phagocytosis of Opa_{52} *Neisseria gonorrhoeae* requires a Src-like tyrosine kinase- and Rac1-dependent signalling pathway. *EMBO J.* **17**, 443-454. doi:10.1093/emboj/17.2.443

Heinrich, A., Heyl, K. A., Klaile, E., Muller, M. M., Klassert, T. E., Wiessner, A., Fischer, K., Schumann, R. R., Seifert, U., Riesbeck, K. et al. (2016). *Moraxella catarrhalis* induces CEACAM3-Syk-CARD9-dependent activation of human granulocytes. *Cell. Microbiol.* **18**, 1570-1582. doi:10.1111/cmi.12597

Hill, D. J. and Virji, M. (2003). A novel cell-binding mechanism of *Moraxella catarrhalis* ubiquitous surface protein UspA: specific targeting of the N-domain of carcinoembryonic antigen-related cell adhesion molecules by UspA1. *Mol. Microbiol.* **48**, 117-129. doi:10.1046/j.1365-2958.2003.03433.x

Janeway, C. A., Jr. and Medzhitov, R. (2002). Innate immune recognition. *Annu. Rev. Immunol.* **20**, 197-216. doi:10.1146/annurev.immunol.20.083001.084359
Kaplan, E., Stone, R., Hume, P. J., Greene, N. P. and Koronakis, V. (2020). Structure of CYRI-B (FAM49B), a key regulator of cellular actin assembly. *Acta Crystallogr. D Struct. Biol.* **76**, 1015-1024. doi:10.1107/S2059798320010906
Kim, J. H., Lee, S. R., Li, L. H., Park, H. J., Park, J. H., Lee, K. Y., Kim, M. K., Shin, B. A. and Choi, S. Y. (2011). High cleavage efficiency of a 2A peptide derived from porcine teschovirus-1 in human cell lines, Zebrafish and mice. *PLoS One* **6**, e18556. doi:10.1371/journal.pone.0018556
Koniger, V., Holsten, L., Harrison, U., Busch, B., Loell, E., Zhao, Q., Bonsor, D. A., Roth, A., Kengmo-Tchoupa, A., Smith, S. I. et al. (2016). *Helicobacter pylori* exploits human CEACAMs via HopQ for adherence and translocation of CagA. *Nat. Microbiol.* **2**, 16188. doi:10.1038/nmicrobiol.2016.188
Kuespert, K., Pils, S. and Hauck, C. R. (2006). CEACAMs - their role in physiology and pathophysiology. *Curr. Opin. Cell Biol.* **18**, 565-571. doi:10.1016/j.ceb.2006.08.008
Kuespert, K., Roth, A. and Hauck, C. R. (2011). *Neisseria meningitidis* has two independent modes of recognizing its human receptor CEACAM1. *PLoS One* **6**, e14609. doi:10.1371/journal.pone.0014609
Kupsch, E.-M., Knepper, B., Kuroki, T., Heuer, I. and Meyer, T. F. (1993). Variable opacity (Opa) outer membrane proteins account for the cell tropisms displayed by *Neisseria gonorrhoeae* for human leukocytes and epithelial cells. *EMBO J.* **12**, 641-650. doi:10.1002/j.1460-2075.1993.tb05697.x
Le, A. H., Yelland, T., Paul, N. R., Fort, L., Nikolaou, S., Ismail, S. and Machesky, L. M. (2021). CYRI-A limits invasive migration through macropinosome formation and integrin uptake regulation. *J. Cell Biol.* **220**, e202012114. doi:10.1083/jcb.202012114
Magoc, T. and Salzberg, S. L. (2011). FLASH: fast length adjustment of short reads to improve genome assemblies. *Bioinformatics* **27**, 2957-2963. doi:10.1093/bioinformatics/btr507
Mccaw, S. E., Schneider, J., Liao, E. H., Zimmermann, W. and Gray-Owen, S. D. (2003). Immunoreceptor tyrosine-based activation motif phosphorylation during engulfment of *Neisseria gonorrhoeae* by the neutrophil-restricted CEACAM3 (CD66d) receptor. *Mol. Microbiol.* **49**, 623-637. doi:10.1046/j.1365-2958.2003.03591.x
Pils, S., Schmitter, T., Neske, F. and Hauck, C. R. (2006). Quantification of bacterial invasion into adherent cells by flow cytometry. *J. Microbiol. Methods* **65**, 301-310. doi:10.1016/j.mimet.2005.08.013
Pils, S., Gerrard, D., Meyer, A. and Hauck, C. R. (2008). CEACAM3: an innate immune receptor directed against human-resticted bacterial pathogens. *Int. J. Med. Microbiol.* **298**, 553-560. doi:10.1016/j.ijmm.2008.04.005
Pils, S., Kopp, K., Peterson, L., Delgado-Tascon, J., Nyffenegger-Jann, N. J. and Hauck, C. R. (2012). The adaptor molecule Nck localizes the WAVE complex to promote actin polymerization during CEACAM3-mediated phagocytosis of bacteria. *PLoS One* **7**, e32808. doi:10.1371/journal.pone.0032808
Roth, A., Mattheis, C., Muenzner, P., Unemo, M. and Hauck, C. R. (2013). Innate recognition by neutrophil granulocytes differs between *Neisseria gonorrhoeae* strains causing local or disseminating infections. *Infect. Immun.* **81**, 2358-2370. doi:10.1128/IAI.00128-13
Rubinson, D. A., Dillon, C. P., Kwiatkowski, A. V., Sievers, C., Yang, L., Kopinja, J., Rooney, D. L., Zhang, M., Ihrig, M. M., Mcmanus, M. T. et al. (2003). A lentivirus-based system to functionally silence genes in primary mammalian cells, stem cells and transgenic mice by RNA interference. *Nat. Genet.* **33**, 401-406. doi:10.1038/ng1117
Sanjana, N. E., Shalem, O. and Zhang, F. (2014). Improved vectors and genome-wide libraries for CRISPR screening. *Nat. Methods* **11**, 783-784. doi:10.1038/nmeth.3047
Sarantis, H. and Gray-Owen, S. D. (2007). The specific innate immune receptor CEACAM3 triggers neutrophil bactericidal activities via a Syk kinase-dependent pathway. *Cell. Microbiol.* **9**, 2167-2180. doi:10.1111/j.1462-5822.2007.00947.x
Sarantis, H. and Gray-Owen, S. D. (2012). Defining the roles of human carcinoembryonic antigen-related cellular adhesion molecules during neutrophil responses to *Neisseria gonorrhoeae*. *Infect. Immun.* **80**, 345-358. doi:10.1128/IAI.05702-11
Schmitter, T., Agerer, F., Peterson, L., Muenzner, P. and Hauck, C. R. (2004). Granulocyte CEACAM3 is a phagocytic receptor of the innate immune system that mediates recognition and elimination of human-specific pathogens. *J. Exp. Med.* **199**, 35-46. doi:10.1084/jem.20030204
Schmitter, T., Pils, S., Sakk, V., Frank, R., Fischer, K. D. and Hauck, C. R. (2007). The granulocyte receptor CEACAM3 directly associates with Vav to promote phagocytosis of human pathogens. *J. Immunol.* **178**, 3797-3805. doi:10.4049/jimmunol.178.6.3797
Shang, W., Jiang, Y., Boettcher, M., Ding, K., Mollenauer, M., Liu, Z., Wen, X., Liu, C., Hao, P., Zhao, S. et al. (2018). Genome-wide CRISPR screen identifies FAM49B as a key regulator of actin dynamics and T cell activation. *Proc. Natl. Acad. Sci. USA* **115**, E4051-E4060. doi:10.1073/pnas.1801340115
Skubitz, K. M., Campbell, K. D. and Skubitz, A. P. (1996). CD66a, CD66b, CD66c, and CD66d each independently stimulate neutrophils. *J. Leukoc. Biol.* **60**, 106-117. doi:10.1002/jlb.60.1.106
Tchoupa, A. K., Schuhmacher, T. and Hauck, C. R. (2014). Signaling by epithelial members of the CEACAM family - mucosal docking sites for pathogenic bacteria. *Cell Commun Signal* **12**, 27. doi:10.1186/1478-811X-12-27
Tchoupa, A. K., Lichtenegger, S., Reidl, J. and Hauck, C. R. (2015). Outer membrane protein P1 is the CEACAM-binding adhesin of *Haemophilus influenzae*. *Mol. Microbiol.* **98**, 440-455. doi:10.1111/mmi.13134
Underhill, D. M. and Ozinsky, A. (2002). Phagocytosis of microbes: complexity in action. *Annu. Rev. Immunol.* **20**, 825-852. doi:10.1146/annurev.immunol.20.103001.114744
Uphoff, C. C. and Drexler, H. G. (2005). Detection of mycoplasma contaminations. *Methods Mol. Biol.* **290**, 13-23. doi:10.1385/1-59259-838-2:013
Vadlamudi, R. K., Li, F., Barnes, C. J., Bagheri-Yarmand, R. and Kumar, R. (2004). p41-Arc subunit of human Arp2/3 complex is a p21-activated kinase-1-interacting substrate. *EMBO Rep.* **5**, 154-160. doi:10.1038/sj.embor.7400079
Yelland, T., Le, A. H., Nikolaou, S., Insall, R., Machesky, L. and Ismail, S. (2021). Structural basis of CYRI-B direct competition with Scar/WAVE complex for Rac1. *Structure* **29**, 226-237.e4. doi:10.1016/j.str.2020.11.003
Yuki, K. E., Marei, H., Fiskin, E., Eva, M. M., Gopal, A. A., Schwartzentruber, J. A., Majewski, J., Cellier, M., Mandl, J. N., Vidal, S. M. et al. (2019). CYRI/FAM49B negatively regulates RAC1-driven cytoskeletal remodelling and protects against bacterial infection. *Nat. Microbiol.* **4**, 1516-1531. doi:10.1038/s41564-019-0484-8